

Phase separation and nanostructuring in the thermoelectric material $\text{PbTe}_{1-x}\text{S}_x$

H. Lin, E. S. Božin and S. J. L. Billinge*

Department of Physics and Astronomy, Michigan State University, East Lansing, MI 48824

J. Androulakis, C. H. Lin and M. G. Kanatzidis

Department of Chemistry, Michigan State University, East Lansing, MI 48824

(Dated: October 9, 2018)

The average and local structures of the $(\text{PbTe})_{1-x}(\text{PbS})_x$ system of thermoelectric materials has been studied using the Rietveld and atomic pair distribution function (PDF) methods. Samples with $0.25 \leq x$ are macroscopically phase separated. Phase separation was suppressed in a quenched $x = 0.5$ sample which, nonetheless, exhibited a partial spinodal decomposition. The promising thermoelectric material with $x = 0.16$ showed intermediate behavior. Combining TEM and bulk scattering data suggests that the sample is a mixture of PbTe rich material and a partially spinodally decomposed phase similar to the quenched 50% sample. This results in a nano-meter scale inhomogeneous material that accounts for its very low thermal conductivity.

PACS numbers: 61.10.-i, 72.15.Jf, 73.50.Lw, 73.63.Bd

I. INTRODUCTION

Thermoelectric materials are the subject of intense research because of their potential for efficient power generation and cooling. The efficiency of the thermoelectric material is measured by the figure of merit, ZT , defined by several interdependent physical parameters.¹ It is difficult to get a high ZT material due to the competing requirements for optimizing the interdependent parameters. Many efforts have focused on reducing the thermal conductivity κ , without sacrificing electrical conductivity, σ . κ is the sum of the lattice thermal conductivity κ_{lat} and the electronic thermal conductivity κ_{ele} . Theoretical and experimental studies suggest that materials that show nano-phase separation appear to be promising in achieving high performance.^{2,3,4,5}

The material with composition $\text{PbTe}_{0.84}\text{S}_{0.16}$ shows a very low room temperature lattice thermal conductivity of 0.4 W/m K and a ZT value significantly higher than that of PbTe and PbS.⁶ The thermal conductivity is only 28% of that observed in the PbTe system, which is remarkable given that the two are isostructural and $\text{PbTe}_{0.84}\text{S}_{0.16}$ has only 16 At. % of S substituted on the Te site. Understanding the origin of this remarkable reduction in κ for a small doping change should give important insights into the thermoelectric problem.

Early studies on the $(\text{PbTe})_{1-x}(\text{PbS})_x$ system showed that phase separation occurs at low temperature over almost the whole composition range.^{7,8} A miscibility gap exists over a wide range of composition and extends almost up to the melting point of the alloy. There are no apparent intermediate compounds and the phase separation occurs into phases which are almost pure PbTe and PbS over the whole alloy range. Theoretical work⁸ supports such a picture and the calculated phase diagram using a thermodynamic model agreed with the previous experimental data. Earlier work^{9,10,11} suggested a smaller range for the miscibility gap in the phase diagram and this discrepancy was attributed to the subtle differ-

ence in chemical processing⁷ and quenching rate. It is apparent from the high resolution transmission electron microscopy (HRTEM) images is that phase separation occurs on several different length-scales in $\text{PbTe}_{0.84}\text{S}_{0.16}$ and that naturally forming striped nanostructures due to spinodal decomposition are evident in portions of the sample. Here we investigate this question further using bulk diffraction probes of the average and local atomic structure. We address two questions. First, can we confirm that the nano-scale phase separation is a bulk property and can we characterize the average chemical composition and structure of the spinodal domain? We have also extended the study to other compositions in the phase diagram to see how these effects evolve with changing composition.

The atomic pair distribution function (PDF) analysis of x-ray diffraction data is a useful method for studying nano-phase separated samples.^{12,13} In the PDF approach both Bragg and diffuse scattering are analyzed and it yields the bulk average local atomic structure. Recently it was successfully used to study the thermoelectric material, $\text{Ag}_x\text{Pb}_m\text{SbTe}_{m+2}$, where silver and antimony rich nano-scale clusters were found to be coherently embedded in the PbTe matrix as a bulk property.¹⁴

We have used both PDF and Rietveld methods to study the $(\text{PbTe})_{1-x}(\text{PbS})_x$ system. We find phase separation occurring over the whole composition range. Refinements from both Rietveld and PDF methods show that the $x = 0.25, 0.5$, and 0.75 samples are macroscopically separated into phases that are almost pure PbS and PbTe. This does not happen in the important 16% PbS doped sample. However, taking all the evidence together we suggest that the 16% sample is a nanoscale mixture of a PbTe rich phase with a partially spinodally decomposed phase of nominally 50% composition. Such a phase was stabilized and observed in a quenched $x = 0.5$ sample in this study. This offers the opportunity in the future for engineering nano- and micro-structures with favorable thermoelectric properties by controlling the thermal

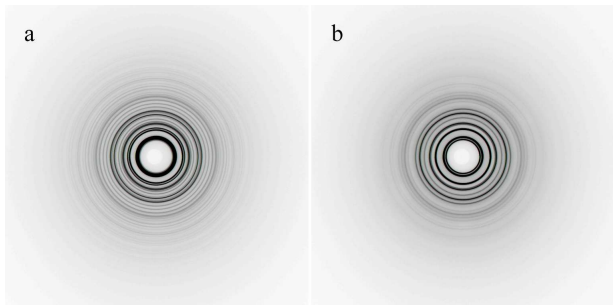


FIG. 1: Raw x-ray powder diffraction data from the 2D detector for the $x = 0.50$ $(\text{PbTe})_{1-x}(\text{PbS})_x$ sample. Data from the (a) unquenched and (b) quenched samples are shown for comparison. The 1-D integrated powder diffraction patterns obtained from these data are shown in Fig. 2(a) and on an expanded scale in Fig. 4. The white circle in the center of each 2D diffractogram represents a shadow from the beam-stop.

history in these materials.

II. EXPERIMENTAL METHODS

Powder samples in the $(\text{PbTe})_{1-x}(\text{PbS})_x$ series were made with different compositions: $x = 0, 0.16, 0.25, 0.50, 0.75$ and 1 . The samples were produced by mixing appropriate ratios of high purity elemental starting materials with a small molar percentage of PbI_2 , an n -type dopant. The initial loads were sealed in fused silica tubes under vacuum and fired at 1273 K for 6 h, followed by rapid cooling to 773 K and held there over a period of 72 h. One $x = 0.5$ sample was also quenched rapidly to room-temperature. More details of sample synthesis can be found elsewhere.⁶

Finely powdered samples were packed in flat plates with a thickness of 1.0 mm sealed between kapton tape windows. X-ray powder diffraction data were collected using the rapid acquisition PDF (RA-PDF) method,¹⁵ which benefits from very high energy x-rays and a two-dimensional detector. The experiments were conducted using synchrotron x-rays with an energy of 86.727 keV ($\lambda = 0.14296$ Å) at the 6-ID-D beam line at the Advanced Photon Source (APS) at Argonne National Laboratory. The data were collected using a circular image plate camera (Mar345) 345 mm in diameter. The camera was mounted orthogonally to the beam path with a sample-to-detector distance of 210.41 mm.

In order to avoid saturation of the detector, each room temperature measurement was carried out in multiple exposures. Each exposure lasted 5 seconds, and each sample was exposed five times to improve the counting statistics. Two representative 2D diffraction images for unquenched and quenched $\text{PbTe}_{0.5}\text{S}_{0.5}$ samples are shown in Fig. 1(a) and (b), respectively. The excellent powder statistics, giving uniform rings, are evident. All the samples yielded similar quality images. The 2D Data sets from each sample were combined and integrated using

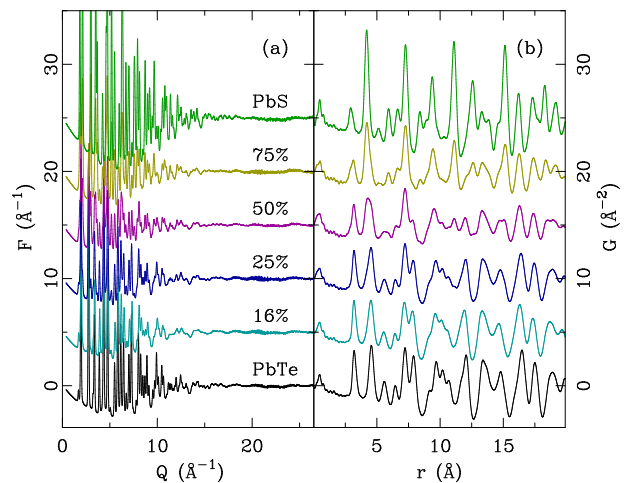


FIG. 2: Experimental (a) $F(Q)$ and (b) $G(r)$ for all unquenched samples. In the Fourier transform, Q_{max} was set to 26.0 Å⁻¹. The data are offset for clarity. The compositions of the $(\text{PbTe})_{1-x}(\text{PbS})_x$ samples are indicated in panel (a). From top to bottom: $x = 1.00$ (green), $x = 0.75$ (yellow), $x = 0.50$ (magenta), $x = 0.25$ (blue), $x = 0.16$ (cyan), and $x = 0.00$ (black).

the program FIT2D¹⁶ before further processing.

Data from an empty container were also collected to subtract the container scattering. The corrected total scattering structure function, $S(Q)$, was obtained using standard corrections^{13,15} with the program PDFgetX2.¹⁷ Finally, the PDF was obtained by Fourier transformation of $S(Q)$ according to $G(r) = \frac{2}{\pi} \int_0^{Q_{max}} Q[S(Q) - 1] \sin(Qr) dQ$, where Q is the magnitude of the scattering vector. A $Q_{max} = 26.0$ Å⁻¹ was used. Fig. 2, shows $F(Q) = Q(S(Q) - 1)$ and $G(r)$ for all the samples. The good statistics and overall quality of the data are apparent in Fig. 2(a). The low spurious ripples at low- r in the $G(r)$ functions are also testament to the quality of the data.¹⁸ Note that $G(r)$ has been plotted all the way to $r = 0$ in these plots, which is a stringent test of this.

III. MODELING

Both PDF (using the PDFfit2 program^{19,20}) and Rietveld²¹ (using the TOPAS program²²) refinements were carried out on the system. The models used in the fits are described below.

One of the main outcomes of this study is to determine the phase composition of the phase-separated sample as a function of composition. When phase separation is long-ranged, Rietveld refinement can be used to estimate the relative abundance of the phase components^{23,24,25,26,27,28}.

Phase segregation can also be determined from the PDF.^{14,29} In PDFfit2, each phase in a multi-phase fit has its own scale-factor in the refinement. The scale factor reflects both the relative phase-fraction of the phases

TABLE I: Refinement results from PbS and PbTe compared with literature values.

	Literature ^a	Rietveld	PDF
R_w	-	0.03994	0.0852
a_{PbTe} (\AA)	6.4541(9)	6.4776(3)	6.465(3)
U_{Pb} (\AA^2)	0.0204(3)	0.033(5)	0.032(4)
U_{Te} (\AA^2)	0.0141(2)	0.009(9)	0.014(4)
R_w	-	0.04377	0.0820
a_{PbS} (\AA)	5.9315(7)	5.9460(3)	5.940(3)
U_{Pb} (\AA^2)	0.0163(3)	0.023(3)	0.0185(5)
U_S (\AA^2)	0.0156(5)	0.018(4)	0.030(5)

^aRef. 30

and the average scattering power of each phase, which depends on the chemical compositions of each phase. The conversion from scale-factor to atomic-fraction is done using the equations derived in Ref. 14.

For each sample, we explored different models. The structure is of the rock-salt type, space group Fm-3m. First we start from a homogeneous (solid solution) model where the anions are assumed to randomly distributed on the sites of the anionic sublattice. In this model, S atoms substitute the Te site randomly without breaking the symmetry. The only structural parameters refined are the lattice constants and the atomic displacement factors.

The next model we tried was a simple two-phase model in which a phase separation into a PbTe-rich and PbS-rich phase was assumed. The phase diagram for this system shows a miscibility gap at low temperature over a wide composition range.^{7,8} The two phases that coexist have compositions rather close to the pure end-members and there is limited solid solubility. Based on this, and in an effort to keep the modeling as simple as possible, we modeled the phase separation as a mixture of pure PbTe and PbS; however, allowing the lattice constants to vary as would be expected if the phases were not the pure end-members. The parameters that were allowed to vary in these fits were lattice constants, atomic displacement factors and phase specific scale factors which reflect the relative abundance of each phase. More complicated phase separated models were also tried where the composition of the phases was varied as described below.

IV. RESULTS

First we carried out PDF and Rietveld refinements on the undoped end-members of the series, PbS and PbTe. The level of agreement of Rietveld and PDFfit refinements can be seen in Fig. 3 and Table I. These fits give a baseline for the quality of the fits for materials without disorder. The fits are acceptable and the refined parameters are in reasonable agreement with literature values for PbTe, though outside the estimated errors. The PDF and Rietveld refinements are also only in semi-quantitative agreement. The parameter estimates were made on the

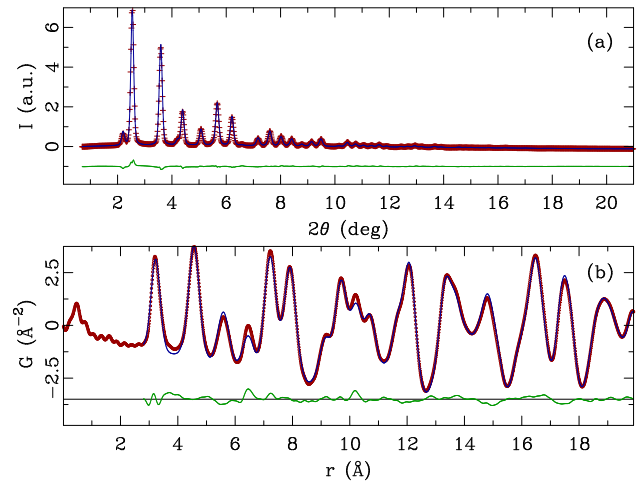


FIG. 3: Representative refinements of the PbTe data using (a) Rietveld and (b) PDF approaches. Symbols represent data, and solid lines are the model fits. The difference curves are offset for clarity.

same data-sets but using different methods and systematic errors are not accounted for in the error estimates. Even in these nominally pure materials the refined atomic displacement factors are rather large³¹, which is in agreement with previous work,³⁰ though this behavior is not really understood.

Now we consider the chemically mixed systems. The existence of phase separation can be *qualitatively* verified in our samples by looking at the diffraction patterns in Fig. 4. The top curve is PbS and the bottom curve is PbTe and the vertical dashed lines are at the positions of the main Bragg-peaks of these phases. Despite the low-resolution of the data, a characteristic of the RAPDF measurement,¹⁵ for compositions $x = 0.25, 0.50$ and 0.75 a coexistence of PbS and PbTe diffraction patterns is clearly evident as the diffraction patterns are qualitatively recognizable as a linear superposition of the end-member patterns. Diffraction peaks appear at precisely the positions of the end-member Bragg-peaks. The same is true for the annealed $x = 0.5$ sample (dark magenta). On the other hand, the *quenched* $x = 0.5$ sample has a diffraction pattern that resembles the PbTe pattern but shifted significantly to higher scattering angles. This is what would be expected for a solid-solution, rather than phase separated, sample suggesting that quenching the sample suppresses phase separation.

The situation is slightly less clear for the $x = 0.16$ sample which resembles closely the pure PbTe diffraction pattern. The effects of phase separation would be difficult to see in this case because of the small PbS component. However, careful inspection of the curve indicates that the main peaks are shifted to higher scattering angles, in analogy with the quenched $x = 0.5$ sample. Thus, this sample appears to be a solid-solution on the macro-scale probed in a diffraction pattern.

We would like to consider evidence in the *local* struc-

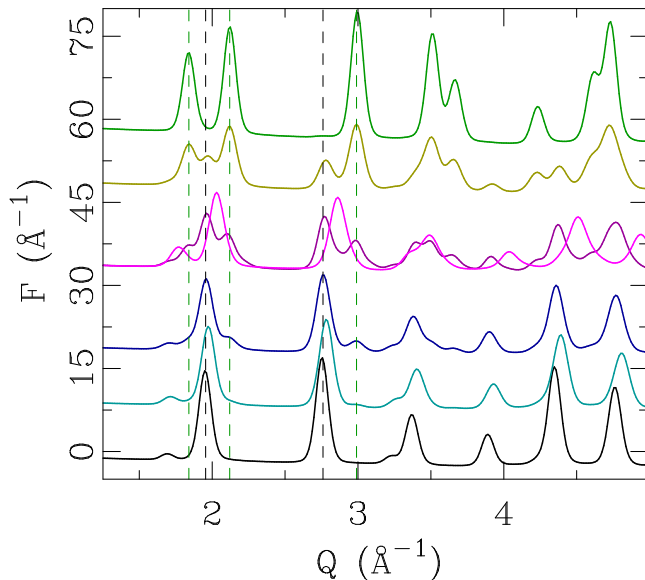


FIG. 4: The low- Q diffraction patterns of all the $(\text{PbTe})_{1-x}(\text{PbS})_x$ samples studied, where $F(Q) = Q(S(Q) - 1)$. From top to bottom: $x = 1.00$ (green), $x = 0.75$ (yellow), $x = 0.50$ (light and dark magenta), $x = 0.25$ (blue), $x = 0.16$ (cyan), and $x = 0.00$ (black). The data corresponding to the quenched $x = 0.50$ sample (light magenta) is superimposed on top of that of the unquenched sample (dark magenta) without being offset. The other data are offset for clarity. Vertical dashed lines indicate positions of several characteristic Bragg peaks in the end-member data to allow for easier comparison.

ture for phase separation. The PDFs of the data in Fig. 4 are shown in Fig. 5 arranged in the same way and with the same colors as in Fig. 4. The samples that are macroscopically phase separated ($x = 0.25, 0.5$ (annealed) and 0.75) also show phase separation in the local structure as expected, the curves having the qualitative appearance of a mixture of the end-member PDFs.

The behavior of peaks in the PDF in solid-solutions has been discussed previously.^{32,33} The nearest neighbor peaks retain the character of the end-members, albeit with a small strain relaxation. However, peaks at higher- r , from the second-neighbor onwards, appear broadened because of inhomogeneous strain in the sample but are peaked at the average position expected from the average structure for the solid solution. The $x = 0.5$ (quenched) and $x = 0.16$ samples follow this behavior even on the 1 nm length-scale suggesting that they are solid-solutions even on the local scale.

To investigate the phase separation phenomenon more quantitatively, we carried out two-phase refinements for the macroscopically phase separated samples on both the diffraction data and the PDF. Fig. 6 shows representative fits from the $x = 0.50$ sample. The refined parameters are reproduced in Table II. In the table the n and n_0 refer to the refined fraction of the sample in the PbTe phase and the expected fraction based on the stoichiometry and assuming phase separation into pure PbTe and

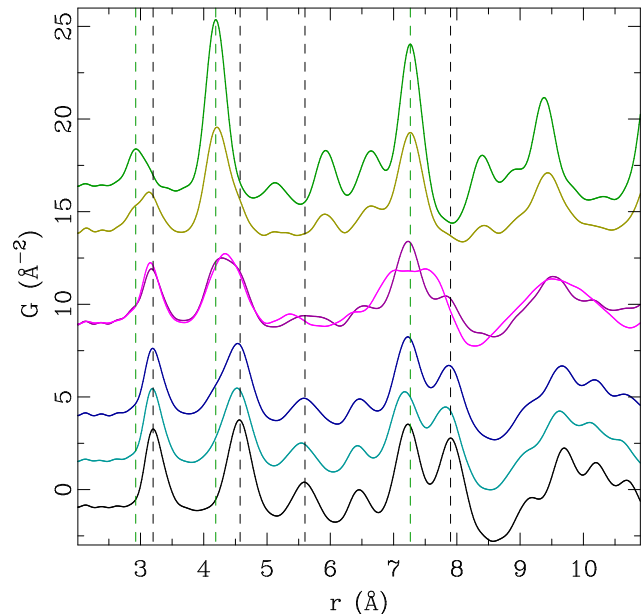


FIG. 5: Experimental PDFs for various $(\text{PbTe})_{1-x}(\text{PbS})_x$ samples on expanded scale. The PDFs, from top to bottom correspond to $x = 1.00$ (green), $x = 0.75$ (yellow), $x = 0.50$ (magenta), quenched $x = 0.50$ (bright magenta), $x = 0.25$ (blue), $x = 0.16$ (cyan), and $x = 0.00$ (black). The data corresponding to the quenched $x = 0.50$ sample (light magenta) is superimposed on top of that of the unquenched sample (dark magenta) without being offset. The other data are offset for clarity. Vertical dashed lines indicate positions of a few selected characteristic PDF features of the end-members for easier comparison.

PbS, respectively. The two-phase fits of pure PbS and PbTe are good (“Rietveld” and “PDF” columns in the table), as indicated by the low residuals. The refined atomic displacement parameters (ADPs) are also in good agreement with the end-member refinements, though the refinements of this parameter are somewhat unstable on the PbS phase when it is the minority phase as it does not contribute strongly to the scattering in that case. The result that relatively large ADPs are needed on the Pb site in PbTe and on the S site in PbS are reproduced in the two-phase fits of the phase separated samples.

The lattice parameters of the PbTe in the phase separated samples are consistently shorter than for the pure material, and they are consistently longer for the PbS phase component. This effect is real and reflects the fact that the phases in the phase separated samples are actually solid-solutions with finite amounts of S in the PbTe and Te in the PbS phase, respectively. We can make a rough estimation of the composition of the phase separated phases by considering their refined lattice parameters and assuming that Vegard’s law^{34,35} is obeyed in the vicinity of the end-member compositions. In this case, the formula for the lattice parameter in the solid solution of composition $\text{PbTe}_{(1-y)}\text{S}_y$ is $a_y = y(a_{\text{PbTe}}) + (1 - y)a_{\text{PbS}}$. Thus, we can estimate the

TABLE II: Refinement results for two-phase fitting to $(\text{PbTe})_{1-x}(\text{PbS})_x$. “Rietveld” and “PDF” refer to Rietveld and PDF fits, respectively, where the composition of the two phases was fixed to PbTe and PbS. n and n_0 refer to the refined and expected (based on stoichiometry) phase fractions for the PbS-rich phase

	$x = 0.25$		$x = 0.5$		$x = 0.75$	
	Rietveld	PDF	Rietveld	PDF	Rietveld	PDF
R_w	0.03427	0.118	0.0468	0.151418	0.03385	0.0996
n/n_0	0.19/0.25	0.20/0.25	0.50/0.50	0.49/0.50	0.71/0.75	0.85/0.75
C	6.4669(3)	6.446(3)	6.4418(3)	6.414(3)	6.4301(3)	6.415(3)
$U_{\text{Pb}} (\text{\AA}^2)$	0.037(6)	0.040(4)	0.041(6)	0.040(5)	0.040(7)	0.040(5)
$U_{\text{Te}} (\text{\AA}^2)$	0.015(6)	0.016(4)	0.0052(6)	0.019(4)	0.033(7)	0.02(4)
$a_{\text{PbS}} (\text{\AA})$	5.9768(3)	5.97(1)	5.9841(3)	5.953(4)	5.9738(3)	5.956(3)
$U_{\text{Pb}} (\text{\AA}^2)$	0.044(8)	0.027(5)	0.034(7)	0.025(4)	0.024(6)	0.023(3)
$U_{\text{S}} (\text{\AA}^2)$	0.073(8)	0.03(5)	-0.0027(7)	0.031(4)	0.0065(6)	0.029(3)

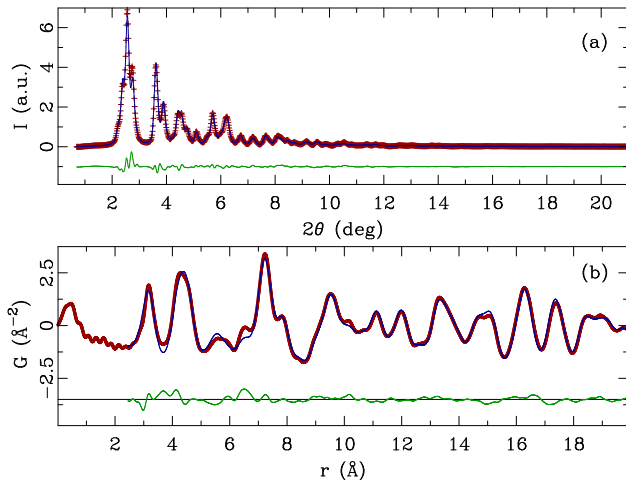


FIG. 6: Representative refinements of the $x = 0.50$ sample data using (a) Rietveld and (b) PDF approach. Symbols represent data, and solid lines are the model fits. The difference curves are offset for clarity.

compositions of the solid-solutions in the phase separated phases from the Rietveld refined lattice parameters. We find that in the $x = 0.25$ phases, $y = 0.94$ for the PbS rich phase and $y = 0.05$ for the PbTe rich phase. This verifies that the composition of the phases in the two-phase mixture are indeed very near PbTe and PbS. The values determined from the $x = 0.5$ and 0.75 samples give nearly the same result with the estimated composition of the PbTe-rich phase as $y = 0.895$ and that of PbS $y = 0.03$. These numbers are consistent with estimates from TEM evidence of a solid solubility limit of 3%.⁶ A more precise determination of these values would be desirable.

The powder diffraction data are relatively insensitive to small changes in chemical composition of the particular phases²⁹ which explains the good fit to the data with the end-member PbS and PbTe compositions, albeit with modified lattice constants. However, for completeness we have carried out two-phase refinements to the phase separated data using the nominal compositions for the two phases that were determined above. The fits were com-

TABLE III: Refinement results from both PDF and Rietveld for the quenched 50% sample from a homogeneous solid-solution model.

	Rietveld	PDF
R_w	0.047	0.163
$a (\text{\AA})$	6.2571(4)	6.217(3)
$U_{\text{Pb}} (\text{\AA}^2)$	0.055(5)	0.062(3)
$U_{\text{Te,S}} (\text{\AA}^2)$	0.017(5)	0.054(3)

parable in quality to those where the composition of the two phases were limited to pure PbTe and PbS, and more physical ADPs were refined on the PbS component.

The agreement of the refined with the nominal composition, n/n_0 , is best in the $x = 0.50$ sample in both the PDF and Rietveld data. It is less good, though acceptable for the 0.25 and 0.75. Due to the relative insensitivity to chemical composition we expect rather large error bars on these quantities and do not ascribe significance to the differences. The agreement between the Rietveld and PDF results shows that the phase separation is macroscopic since we get the same result in both the local and average structures.

We now consider the samples that appear from the qualitative analysis of the data to be solid-solutions: $x = 0.5$ (quenched) and $x = 0.16$. In Fig. 7 we consider the $x = 0.5$ sample. In this figure, model PDFs of the undoped end-members are reproduced for reference and the positions of their main peaks are marked. The quenched data are shown as grey symbols in the curves (c) and the annealed data in the curves (d). The magenta lines are simulated PDFs. In (c) the simulated PDF is from a homogeneous solid-solution virtual-crystal model with the right nominal composition and lattice parameter. It agrees well with the data. In (d) the simulated PDF is a linear combination of the PbTe and PbS PDFs. In each case the ADPs of the simulations have been adjusted to give the best agreement with the data. The simulations fit rather well indicating that this picture of phase separation (annealed) vs solid solution (quenched) is a good explanation of the bulk behavior for the $x = 0.5$ sample. Quantitative refinement results for the quenched 50% sample are reproduced in Table III The fits are good

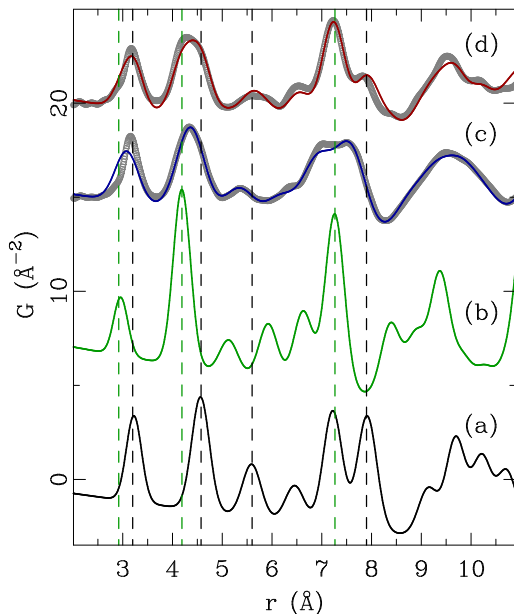


FIG. 7: PDFs of converged models for (a) $x = 0.00$ and (b) $x = 1.00$ $(\text{PbTe})_{1-x}(\text{PbS})_x$ samples. Comparison of the data for (c) quenched and (d) unquenched $x = 0.50$ samples (open symbols) with the solid solution (c) and mixture (d) models (solid lines), respectively. See text for details. Vertical dashed lines indicate positions of selected PDF features characteristic for the end-member compositions, for easier comparison.

with low R_w 's and reasonable refined parameters. The refined lattice parameter is between the end-member values as expected and the ADP on the Pb-site is further enlarged from the end-member values as expected due to disorder in the alloy.

In the quenched $x = 0.5$ sample the solid-solution is not thermodynamically stable but is metastably trapped by the rapid quench. The quench is mostly successful at suppressing phase separation as discussed above. However, it is not completely successful, as TEM images of the quenched $x = 0.5$ sample indicate that the sample has compositional modulations, as shown in Fig. 8(b). The striped nature of these modulations suggests that there is an arrested spinodal decomposition taking place in the 50% doped sample, that would result in sinusoidal compositional modulations about the nominal 50% composition. The amplitude of the modulations is not known, but the good agreement of the homogeneous solid-solution model to the PDF and Rietveld data suggest that the variation in composition around the nominal 50% is not too large.

Thus we understand the quenched 50% sample to be close to an ideal metastable solid solution, but with an arrested spinodal decomposition that gives rise to nano-scale compositional modulations. The extent of the spinodal decomposition in the quenched $x = 0.5$ sample is difficult to assess.

Of greater interest from both a technological and scientific viewpoint is the behavior of the $x = 0.16$ sample that

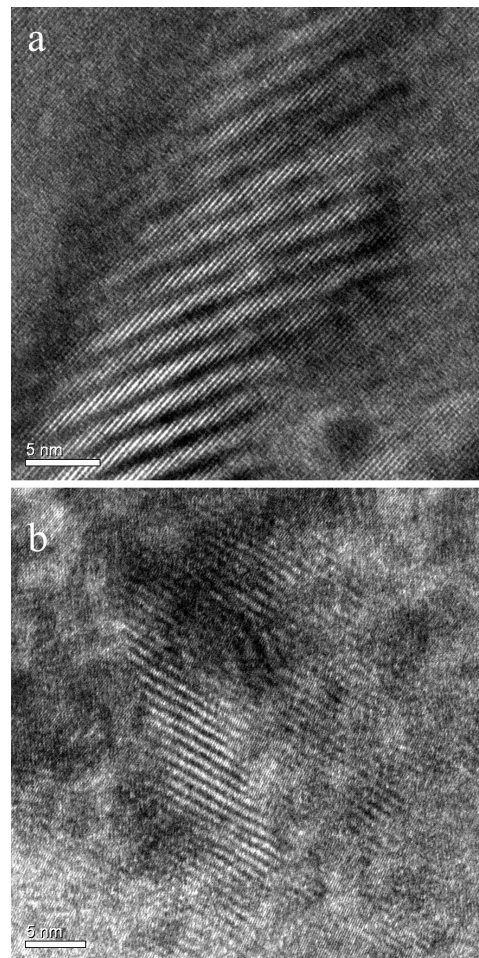


FIG. 8: HRTEM images of (a) $x = 0.16$ and (b) quenched $x = 0.50$ $(\text{PbTe})_{1-x}(\text{PbS})_x$ samples.

shows especially good thermoelectricity. As discussed above, the diffraction data in Fig 4 suggests that the sample is macroscopically a solid solution even though it lies outside the range of solid solubility suggested by the phase diagrams^{7,8} and inferred from the composition of the PbTe-rich phase of the phase-separated compositions in our own refinements (25%, 50%, 75% sample).

We tried fitting two-phase and homogeneous models to both the diffraction and PDF data. The results are shown in Table IV with representative fits shown in Fig. 9. As expected from the qualitative analysis of the data discussed above, the single-phase solid-solution model (model A) provides acceptable fits to the data. The refined lattice parameters are shorter than pure PbTe. According to the Vegard's law analysis, the refined lattice parameter gives a nominal composition for this sample of 0.14 (Rietveld)/0.12(PDF), in reasonable agreement with the actual composition. Enlarged ADPs are found on the Pb sublattice with smaller ADPs on the Te lattice, as was the case for the PbTe end-member. As expected for a solid-solution, the ADPs are enlarged with respect to PbTe.

TABLE IV: Rietveld and PDF refinement results from three different models for the $\text{PbTe}_{0.84}\text{S}_{0.16}$ sample: model A is solid solution model, model B is a simple two-phase mixture of PbTe and PbS and model C is a mixture of pure PbTe phase plus a solid solution of composition $\text{PbTe}_{0.5}\text{-PbS}_{0.5}$. n and n_0 refer to the refined and expected (based on stoichiometry) phase fractions for the PbS-rich phase.

		model A		model B		model C	
		Rietveld	PDF	Rietveld	PDF	Rietveld	PDF
	R_w	0.04647	0.1209	0.05186	0.121	0.03068	0.114
	n/n_0	—	—	0.14/0.16	0.037/0.16	0.31/0.32	0.24/0.32
PbTe	a (Å)	6.4264(5)	6.403(3)	6.4233(4)	6.403(24)	6.4203(4)	6.416(3)
	U_{Pb} (Å ²)	0.047(5)	0.047(3)	0.035(6)	0.035(3)	0.028(6)	0.036(4)
	U_{Te} (Å ²)	0.0061(6)	0.019(3)	0.023(6)	0.029(4)	0.016(6)	0.025(5)
second phase	a (Å)	—	—	5.900(1)	5.942(4)	6.1673(3)	6.255(3)
	U_{Pb} (Å ²)	—	—	0.018(8)	0.021(6)	0.253(8)	0.064(6)
	$U_{\text{S,Te}}$ (Å ²)	—	—	0.013(8)	-0.0024(6)	0.253(8)	0.070(6)

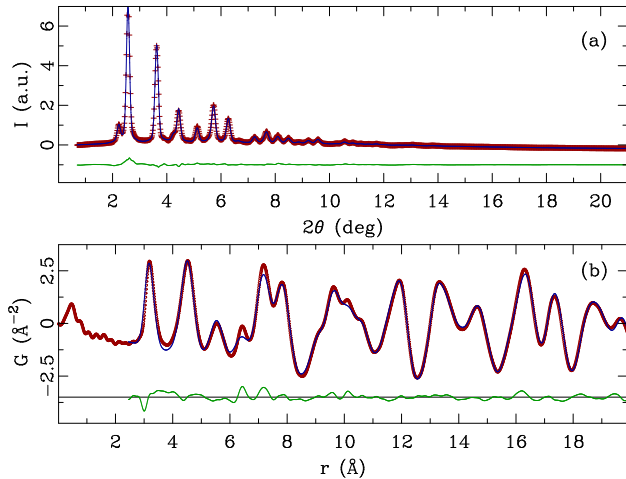


FIG. 9: Representative refinements of the $x = 0.16$ sample data using (a) Rietveld and (b) PDF approach. Symbols represent data, and solid lines are the model fits. The difference curves are offset for clarity.

For completeness, we also tried the simple model of phase separation into pure PbTe and PbS end-members. The results appear in Table IV as model B. The Rietveld fit is significantly worse as measured by R_w . In the case of the PDF fit the R_w is comparable but the refinement reduced the phase fraction of the second phase and adjusted the lattice parameter of the majority phase, moving the refinement back towards the solid-solution result. This refinement also returned unphysical negative atomic displacement factors on the minority phase. The solid-solution model is clearly preferred over full phase separation from the bulk diffraction measurements.

The TEM images from the 16% sample (Ref. 6 and Fig. 8(a)) suggest that it is two-phased, with one phase being homogeneous and the other resembling the quenched $x = 0.5$ sample with arrested spinodal decomposition. A model that simulated this situation was successful compared to the PDF data, as shown from model C in Table IV. This model assumed that the nominally 16% sample is phase separated into regions that are pure

PbTe and regions that resemble the quenched 50% sample, i.e., they are nominally $x = 0.5$ solid-solutions but also exhibiting spinodal decomposition as suggested by the TEM images. Thus, model C is a phase separation into pure PbTe and a solid solution of composition $\text{PbTe}_{0.5}\text{S}_{0.5}$. This model gives the lowest R_w 's for fits to the 16% compound in both the Rietveld and PDF refinements. The phase fractions were free to vary but refined to values that are close to those expected. The lattice constants refined to reasonable values. The majority phase lattice constant was close to that of the PbTe rich phase in the two-phase refinements in Table II. In the case of the minority phase, the lattice constant lay between pure PbTe and PbS consistent with a nominal 50% composition. The ADPs are slightly large in the PbTe-rich phase but physically reasonable. In the minority phase the ADPs are unphysical in the Rietveld refinement suggesting that this parameter is not well determined in the refinement. However, in the PDF refinement they are more reasonable, but very large. This is perfectly consistent with the fact that this minority phase itself actually has a compositional variation due to the spinodal effects.

V. SUMMARY

This work confirmed the phase separation tendency of the PbTe/PbS system. It also showed that phase separation can be effectively, but not completely, suppressed by quenching at 50% composition, where a partial spinodal decomposition appears to be taking place, at least in a portion of the sample.

However, the main result is an improvement in our understanding of the state of the thermoelectrically promising 16% sample. Measurements of the bulk average structure, and the bulk local structure, indicate that it is not phase separated into PbTe-rich and PbS-poor end-members like the other similarly processed samples in the series. The best explanation of all the data at hand is that this sample prefers a phase separation into a PbTe-rich phase and a phase that is nominally 50% doped, but

which has a partial spinodal decomposition reminiscent of the quenched 50% sample. Such a nano-scale phase separation is thought to be important in producing the very low lattice thermal conductivity κ that is observed in this material⁶. Interestingly, in this case the effect appeared not after a quench, but after an anneal, suggesting that it is the thermodynamically preferred state, though this needs to be investigated further. Also of interest is to explore further the nature of the PbTe-rich component, which preliminary TEM investigations⁶ indicate also contains nanostructured regions with nano-scale nuclei of a second phase present.

The other important observation from this work is that quenching is very important in determining the phase separation and resulting nano-scale microstructure. This suggests that in this system it may be possible to engineer κ , and therefore ZT in the bulk material by appropriate heat treatments. This is a promising route for future research.

Acknowledgments

We are grateful to Douglas Robinson for kind help with the experimental setup. We acknowledge Pavol Juhas, Ahmad Masadeh, HyunJeong Kim, and Asel Sartbaeva for their valuable assistance with the data collection. This work was supported in part by National Science Foundation (NSF) grant DMR-0304391 and by the Office of Naval Research. Data were collected at the 6IDD beamline in the Midwest Universities Collaborative Access Team (MUCAT) sector at the Advanced Photon Source (APS). Use of the Advanced Photon Source was supported by the U. S. Department of Energy, Office of Science, Office of Basic Energy Sciences, under Contract No. DE-AC02-06CH11357. The MUCAT sector at the APS is supported by the U.S. DOE, Office of Science, Office of Basic Energy Sciences, through the Ames Laboratory under Contract No. W-7405-Eng-82.

* Electronic address: billinge@pa.msu.edu;
URL: <http://nirt.pa.msu.edu/>

- ¹ $ZT = \sigma S^2 T / \kappa$, where T is the operating temperature of the device, S is the thermopower, and σ and κ are the electrical and thermal conductivities of the material, respectively.
- ² T. C. Harman, P. J. Taylor, M. P. Walsh, and B. E. LaForge, *Science* **297**, 2229 (2002).
- ³ T. C. Harman, M. P. Walsh, B. E. LaForge, and G. W. Turner, *J. Electron Microsc.* **34**, L19 (2005).
- ⁴ K. F. Hsu, S. Loo, F. Guo, W. Chen, J. S. Dyck, C. Uher, T. Hogan, E. K. Polychroniadis, and M. G. Kanatzidis, *Science* **303**, 818 (2004).
- ⁵ W. Kim, J. Zide, A. Gossard, D. Klenov, S. Stemmer, A. Shakouri, and A. Majumdar, *Phys. Rev. Lett.* **96**, 045901 (2006).
- ⁶ J. Androulakis, C. H. Ling, R. Pcionek, H. Kong, C. Uher, T. Hogan, B. Cook, T. Caillat, K. M. Paraskevopoulos, and M. G. Kanatzidis, submitted (2006).
- ⁷ M. S. Darrow, W. B. White, and R. Roy, *T. Metall. Soc. AIME* **236**, 654 (1966).
- ⁸ V. Leute and N. Volkmer, *Z. Phys. Chem. Neue Fol.* **144**, 145 (1985).
- ⁹ S. Yamamoto, *Sci. Rep. Res. Tohoku U., First Ser.* **40**, 11 (1956).
- ¹⁰ N. D. Sindeyeva and A. A. Godovikov, *Dokl. Akad. Nauk SSSR* **127**, 431 (1959).
- ¹¹ A. Y. Malevskiy, *Dokl. Akad. Nauk SSSR* **152**, 191 (1963).
- ¹² S. J. L. Billinge and M. G. Kanatzidis, *Chem. Commun.* pp. 749–760 (2004).
- ¹³ T. Egami and S. J. L. Billinge, *Underneath the Bragg peaks: structural analysis of complex materials* (Pergamon Press, Elsevier, Oxford, England, 2003).
- ¹⁴ H. Lin, E. S. Božin, S. J. L. Billinge, E. Quarez, and M. G. Kanatzidis, *Phys. Rev. B* **72**, 174113 (2005).
- ¹⁵ P. J. Chupas, X. Qiu, J. C. Hanson, P. L. Lee, C. P. Grey, and S. J. L. Billinge, *J. Appl. Crystallogr.* **36**, 1342 (2003).
- ¹⁶ A. P. Hammersley (1998), ESRF Internal Report ESRF98HA01T.
- ¹⁷ X. Qiu, J. W. Thompson, and S. J. L. Billinge, *J. Appl.*

- Crystallogr.* **37**, 678 (2004).
- ¹⁸ P. F. Peterson, E. S. Božin, T. Proffen, and S. J. L. Billinge, *J. Appl. Crystallogr.* **36**, 53 (2003).
- ¹⁹ C. L. Farrow, P. Juhas, J. W. Liu, D. Bryndin, J. Bloch, T. Proffen, and S. J. L. Billinge, *J. Phys: Condens. Matter* (2006), submitted.
- ²⁰ T. Proffen and S. J. L. Billinge, *J. Appl. Crystallogr.* **32**, 572 (1999).
- ²¹ H. M. Rietveld, *J. Appl. Crystallogr.* **2**, 65 (1969).
- ²² A. A. Coelho (2004), TOPAS General Profile and Structure Analysis Software for Powder Diffraction Data; <http://members.optusnet.com.au/~alancoelho/>.
- ²³ P. E. Werner, S. Salome, G. Malmros, and J. O. Thomas, *J. Appl. Crystallogr.* **12**, 107 (1979).
- ²⁴ R. J. Hill and C. J. Howard, *J. Appl. Crystallogr.* **20**, 467 (1987).
- ²⁵ D. L. Bish and S. A. Howard, *J. Appl. Crystallogr.* **21**, 86 (1988).
- ²⁶ B. H. O'Connor and M. D. Raven, *Powder Diffr.* **3**, 2 (1988).
- ²⁷ R. J. Hill, *Powder Diffr.* **6**, 74 (1991).
- ²⁸ R. A. Young, *The Rietveld Method*, vol. 5 of *International Union of Crystallography Monographs on Crystallography* (Oxford University Press, Oxford, 1993).
- ²⁹ T. Proffen, V. Petkov, S. J. L. Billinge, and T. Vogt, *Z. Kristallogr.* **217**, 47 (2002).
- ³⁰ Y. Noda, K. Masumoto, S. Ohba, Y. Saito, K. Toriumi, Y. Iwata, and I. Shibuya, *Acta Crystallogr. C* **43**, 1443 (1987).
- ³¹ I.-K. Jeong, T. Proffen, F. Mohiuddin-Jacobs, and S. J. L. Billinge, *J. Phys. Chem. A* **103**, 921 (1999).
- ³² V. Petkov, I.-K. Jeong, J. S. Chung, M. F. Thorpe, S. Kycia, and S. J. L. Billinge, *Phys. Rev. Lett.* **83**, 4089 (1999).
- ³³ I.-K. Jeong, F. Mohiuddin-Jacobs, V. Petkov, S. J. L. Billinge, and S. Kycia, *Phys. Rev. B* **63**, 205202 (2001).
- ³⁴ L. Vegard, *Z. Phys.* **5**, 17 (1921).
- ³⁵ M. F. Thorpe and E. J. Garboczi, *Phys. Rev. B* **42**, 8405 (1990).